

DBS-relevant electric fields increase hydraulic conductivity of *in vitro* endothelial monolayers

S V Lopez-Quintero, A Datta, R Amaya, M Elwassif, M Bikson and J M Tarbell

Department of Biomedical Engineering, The City College of New York of CUNY, Room T-403b, Steinman Hall, 160 Convent Avenue, New York, NY 10031, USA

E-mail: bikson@ccny.cuny.edu

Received 10 August 2009

Accepted for publication 18 December 2009

Published 14 January 2010

Online at stacks.iop.org/JNE/7/016005

Abstract

Deep brain stimulation (DBS) achieves therapeutic outcome through generation of electric fields (EF) in the vicinity of energized electrodes. Targeted brain regions are highly vascularized, and it remains unknown if DBS electric fields modulate blood–brain barrier (BBB) function, either through electroporation of individual endothelial cells or electro-permeation of barrier tight junctions. In our study, we calculated the intensities of EF generated around energized Medtronic 3387 and 3389 DBS leads by using a finite element model. Then we designed a novel stimulation system to study the effects of such fields with DBS-relevant waveforms and intensities on bovine aortic endothelial cell (BAEC) monolayers, which were used as a basic analog for the blood–brain barrier endothelium. Following 5 min of stimulation, we observed a transient increase in endothelial hydraulic conductivity (L_p) that could be related to the disruption of the tight junctions (TJ) between cells, as suggested by zonula occludens-1 (ZO-1) protein staining. This ‘electro-permeation’ occurred in the absence of cell death or single cell electroporation, as indicated by propidium iodide staining and cytosolic calcein uptake. Our *in vitro* results, using uniform fields and BAEC monolayers, thus suggest that electro-permeation of the BBB may occur at electric field intensities below those inducing electroporation and within intensities generated near DBS electrodes. Further studies are necessary to address potential BBB disruption during clinical studies, with safety and efficacy implications.

1. Introduction

Deep brain stimulation, an invasive electrotherapy considered for the treatment of Parkinson’s disease, tremors, depression, obsessive compulsive disorder, addiction and obesity, targets abnormal neuronal function by generation of high-intensity electric fields near the stimulating electrodes (Bekar *et al* 2008, Benabid 2007, Hardesty and Sackeim 2007, Larson 2008, Lipsman *et al* 2007, Sani *et al* 2007, Tir *et al* 2007, Voges *et al* 2007). Therapeutic actions are considered to be mediated through polarization of neuronal membranes and resulting changes in action potential generation. Current safety considerations for DBS stimulus parameters contemplate electrochemical interaction at the electrode–tissue interface

(Merrill *et al* 2005) and gross undesired behavioral or cognitive changes suffered by patients after implantation (Drapier *et al* 2008). Histological data from deceased DBS subjects have evidenced tissue damage and presence of macrophages in the vicinity of the electrode accompanying glial and foreign body giant cell encapsulation of the DBS lead (Moss *et al* 2004, Sun *et al* 2008, Kuyck *et al* 2007). Widespread damage mechanisms have also been proposed resulting from blunt axonal destruction (Gluckman *et al* 1996). Disruption of local brain micro-vasculature during surgery seems similarly inevitable (Chou *et al* 2007), given an average capillary density of several hundreds per millimeter square of tissue, depending on the brain region (Jensen *et al* 2006) and a lead length of 1.5 mm and a diameter of 1.27 mm for the Medtronic models

used in DBS (Moss *et al* 2004) inserted through a few millimeters of tissue (McClelland *et al* 2009). Furthermore, the EF generated during DBS may alter BBB integrity, but to our knowledge this issue has not been investigated thoroughly.

Electric fields have also been used in electroporation where stimulation has been shown to polarize the lipid cell membrane causing it to become more porous and permeable to otherwise membrane impermeant agents. Previous *in vitro* experiments have shown that with the application of adequate EF, it is possible to cause pores in the cell membrane and deliver molecules inside the cytosol without compromising cell viability, through reversible electroporation (Stacey *et al* 2003, Pucihar *et al* 2007, Rebersek *et al* 2007, Khine *et al* 2007). This well-established technique has been used for cytosolic RNA and DNA electrotransfer, and it is currently being investigated for applications where a therapeutic agent is delivered to the cell or tissue, including cancer drug therapy (electro-chemotherapy). Irreversible electroporation leads to necrosis at higher electric stimulation intensities.

Even though the electric field intensities typically applied in electroporation experiments are higher than those generated during DBS, one cannot rule out the possibility that DBS-relevant EF cause electroporation, since several factors may contribute to the reduction of the electroporation threshold during DBS: (1) an increase in both the number and frequency of electric pulses reduces the threshold (Anwar and Weiss 1989); DBS generally employs 100–185 Hz pulses continuously (e.g. >100 000 pulses every hour) compared to just 1–10 pulses at ~1 Hz in typical electroporation protocols; (2) structural organization of cells and tissue and membrane surface conditions, for example electroporation threshold is higher for cells in suspension (Yang *et al* 1995); (3) a collateral effect of DBS-relevant EF on the cells, for example in the case of barrier tissues such as the blood–brain barrier; ‘electro-permeation’ of the barriers, through disruption of tight junctions, may occur independently of single cell membrane electroporation. This last proposition is specifically tested in this study for DBS-relevant electric fields using an *in vitro* barrier analog.

The integrity of the BBB is essential for maintaining homeostasis in the brain and the central nervous system (CNS), since it constitutes its first line of defense. The BBB is a strict and selective ‘gate’ formed by pericytes, astrocytes, neurons, extracellular matrix and endothelial cells, the latter conferring the barrier property to the structure due to the presence of tight junctions between cells at the apical side (Hawkins and Davis 2005). Therefore, it seems necessary to consider the effect of DBS on endothelial integrity and viability.

To begin to address this concern, we first determined the relevant values of EF in the vicinity of energized Medtronic 3387 and 3389 DBS leads by using a three-dimensional finite element model with brain tissue modeled as a homogeneous cylinder. We then cultured BAEC monolayers that were used as an analog for the BBB endothelium and measured the change in water flux (hydraulic conductivity), as they were stimulated by a uniform field with clinical DBS-relevant waveforms and intensities found from the finite element

model. Immunostaining of a tight-junction protein ZO-1 (zonula occludens-1) was used to assess the integrity of the inter-endothelial junctions. Electroporation and cell viability were determined by calcein uptake and PI (propidium iodide) staining, respectively.

2. Materials and methods

2.1. Chemicals and materials

The following chemicals were obtained from Sigma-Aldrich Chemical Company (St Louis, MO): bovine serum albumin (30% solution), minimum essential medium eagle (MEM), phenol red-free MEM (PF), penicillin–streptomycin solution, L-glutamine, trypsin–EDTA solution, HEPES, sodium bicarbonate, heparin (sodium salt, grade I-A, 181 USP units/mg), triton X-100 and fibronectin. Fetal bovine serum (FBS) was purchased from Hyclone Laboratories (Logan, UT). Paraformaldehyde, Dulbecco’s PBS (1× without Ca²⁺ and Mg²⁺) and PBS (10×) were obtained from Fisher Scientific (Houston, TX). Rabbit anti-ZO-1, Alexa Fluor® 488 donkey anti-rabbit IgG and propidium iodide, impermeant calcein C-481 and cell-permeant calcein C-1430 from Invitrogen (Carlsbad, CA). Transwell polyester filters (24.5 mm diameter, 0.4 μm pore size) were purchased from Costar (Cambridge, MA). Ag/AgCl disc electrodes having a diameter of 8 mm and thickness of 1 mm were purchased from A-M Systems Inc. (Carlsborg, WA).

2.2. Model of EF distribution in brain tissue

In order to determine the EF generated near energized DBS electrodes, a three-dimensional finite element model was implemented in COMSOL Multiphysics 3.5 (COMSOL Inc., Burlington, MA) as previously described (Elwassif *et al* 2006).

We modeled two different Medtronic DBS leads, the 3387 DBS lead with a 1.5 mm spacing between each of the four electrodes resulting in an electrode spread over a total of 10.5 mm, and the 3389 DBS lead with a 0.5 mm spacing between each of four electrodes resulting in an electrode spread over a total of 7.5 mm. The brain tissue was modeled as a cylinder with 2.5 cm radius and 5 cm height with homogeneous electrical conductivity $\sigma = 0.3 \text{ S m}^{-1}$ (figure 1). For each lead, we energized either electrodes 1 and 2 (the two most proximal) or electrodes 1 and 4 (the two most distal). The electrical potential of the active electrode was set to 3 V (electrode 1), the ground potential boundary conditions were applied to electrode 2 or 4 as shown in figure 1 and all other boundaries were electrically insulated ($n \cdot J = 0$).

Because of axial geometrical symmetry, the same geometrical and electrical properties for the 3D model as for the axisymmetric model were used. The governing equations for steady currents were used to calculate the electric field around the electrodes (following the quasi-static assumption). The current in the domain is controlled by a continuity equation, which follows from the Maxwell equation:

$$\nabla \cdot \vec{J} = -\nabla \cdot (\sigma \nabla V) = 0$$

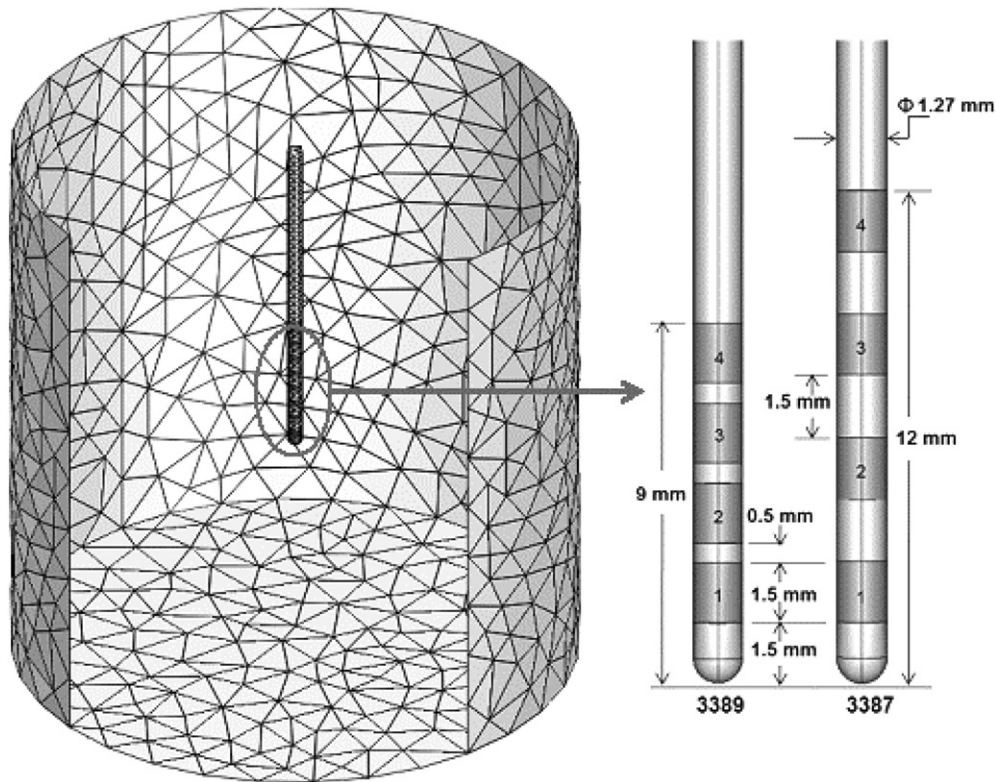


Figure 1. Schematic diagram of the 3D finite element model, geometry and mesh configuration. Brain tissue was modeled as a cylinder (radius = 2.5 cm and height = 5 cm). The bottom of the DBS lead was positioned at the center of the tissue (encircled region). Two DBS leads were modeled: the 3389 DBS lead with 1.5 mm electrodes and 0.5 mm spacing between electrodes and 3387 DBS with 1.5 mm electrodes and 1.5 mm spacing (right). A typical configuration (3 V) was applied in the homogeneous brain tissue with electrical conductivity of $\sigma = 0.3 \text{ S m}^{-1}$ (see section 2). The induced local electric field in the tissue was calculated numerically using the finite element model.

where J is the current density (A m^{-2}), defined as $J = \sigma E$ and $E = -\nabla V$ (Laplace's equation), σ is the electrical conductivity (S m^{-1}), E is the electric field (V m^{-1}) and V is the electrical potential.

2.3. Bovine aortic endothelial cell culture

BAEC were purchased from VEC Technologies (Rensselaer, NY) and grown in T-75 flasks with 10% FBS-MEM. The flasks were incubated at 37°C and 5% CO_2 . Upon confluence (3–4 days), the cells were split to continue maintenance of the cell line.

2.4. Bovine aortic endothelial cells insert preparation

In order to have a model for the endothelium, BAEC were plated at a density of $1.25 \times 10^5 \text{ cells cm}^{-2}$ on fibronectin-coated Transwell polyester filters and then were incubated at 37°C in 5% CO_2 and 10% FBS-MEM. The permeability experiments were run 6–8 days after plating, once the cells were totally confluent but free from overgrowth. Cells were used from passages 5 to 8. These methods have been well documented in previous studies (Cancel *et al* 2007, Chang *et al* 2000, DeMaio *et al* 2004)

2.5. Determination of the water flux across the endothelium

The measurement of the water flux across the BAEC monolayer supported on the Transwell filter was performed with an apparatus developed in our lab and used previously in several studies to measure hydraulic conductivity (Chang *et al* 2000, DeMaio *et al* 2004, Lakshminarayanan *et al* 2000, Sill *et al* 1995). The apparatus (figure 2) was kept inside a Plexiglas hood and maintained at 37°C . The seeded filters were sealed inside an acrylic chamber to form a luminal (top) compartment that was completely isolated from the abluminal (bottom) compartment. The latter was connected to a reservoir via Tygon and borosilicate glass tube. The vertical displacement of the reservoir fluid level with respect to the liquid covering the cells allowed us to apply a hydrostatic pressure differential across the monolayer. When a 10 cm H_2O differential pressure was applied, the water flux J_v/A (cm s^{-1}), where J_v is the volumetric flow rate across the monolayer and A is the area of the monolayer, was measured by tracking the position of a bubble that was inserted into the borosilicate glass tube. The bubble displacement data were acquired through BT-Millennium software and used to compute the J_v/A values every 5 min.

During the entire experiment, the luminal compartment and the reservoir were fed with gas (5% CO_2 –95% balanced air) to maintain the experimental media at the physiological

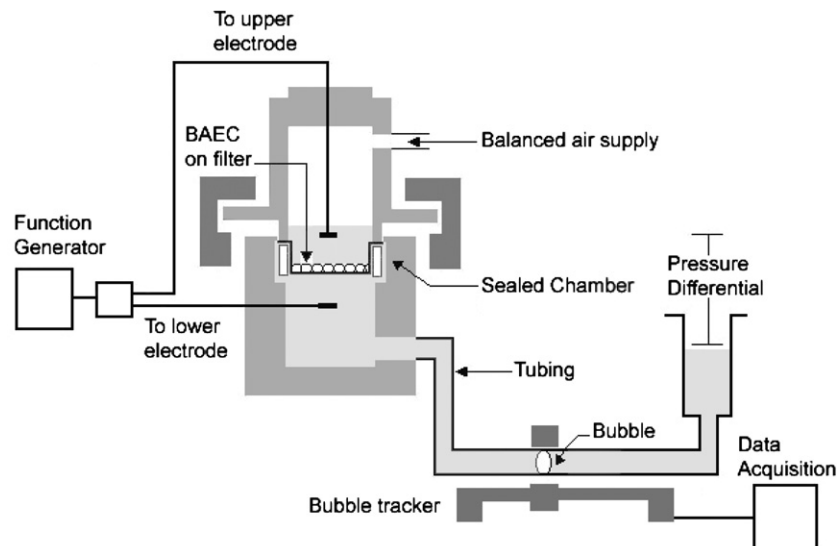


Figure 2. Schematics of the novel experimental setup used to apply an electric field to the BAEC monolayers and measure the water flux across them. The filters were placed inside the chamber and the water flux was measured after the application of a 10 cm H₂O pressure differential. The BAEC monolayers were then stimulated for 5 min using a function generator so that the final EF were 62.5 V m⁻¹, 125 V m⁻¹ and 250 V m⁻¹. After stimulation with the EF, we observed the changes in the water flux across the monolayer.

pH of 7.4. Toward the end of the first hour (at $t = 60$ min), an electric field was applied for 5 min and its effect on the water flux was observed during the next 2 h. The experiment lasted a total of 3 h.

It is worth noticing that the initial measurement of the water flux for 55 min is important to characterize the monolayers before the electric field application. Monolayers that were leaky and presented defects were discarded.

2.6. Electric field application

Unless otherwise stated, stimulation of the BAEC monolayer was performed using a programmable function generator (Model AFG 320, Tektronix) and an analog stimulus isolator (Model 2200, A-M Systems) connected to two 8 mm Ag/AgCl electrodes placed across the cell monolayer. One electrode was placed 2 cm below the monolayer and the other one 2 cm above (figure 2) to ensure application of a uniform electric field across the cell monolayer (Datta *et al* 2007). Ag/AgCl electrodes, commonly used for *in vitro* (brain slice) stimulation studies, were selected for their charge passing capacity, to minimize irreversible electrochemical reactions (Merrill *et al* 2005). The function generator was programmed to generate a typical DBS biphasic charge-balanced waveform. The anodic pulse begins ~ 0.4 ms after the end of the cathodic pulse and ends ~ 4 ms before the beginning of the next cathodic pulse (Butson and McIntyre 2005; Elwassif *et al* 2006). The duration of both pulses (anodic and cathodic) was 90 μ s and the amplitude varied from 0.25 V to 1 V. The isolator amplified the signal from the function generator tenfold, so that the voltage applied ranged from 2.5 V to 10 V for a final electric field ranging from 62.5 V m⁻¹ to 250 V m⁻¹. A pair of electrodes was not used more than seven times to avoid electrochemical damage (Merrill *et al* 2005).

The central premise underlying our methodology has been applied in previous *in vitro* DBS studies (including by our group: Bikson *et al* 2001, 2004, Radman *et al* 2007) and the rationale was as follows. It is well established that DBS affects changes in the surrounding tissue by the induction of extracellular voltages; moreover, individual cell membrane polarization (activation) is determined by the *local* intensity of extracellular voltage, which decays with distance from the electrode (Yousif and Liu 2007). For endothelial cells in the presence of induced extracellular voltages, membrane polarization may cause changes in blood–barrier function. To address the hypothesis that DBS-relevant electric fields induce changes in blood–barrier function through direct (not neuronal mediated) action, we designed an experimental setup that allows the application of precisely controlled (uniform) electric fields to endothelial cell monolayers. The purpose of our FEM analysis is to determine the local electric fields at specific distances from the electrode (e.g. where a blood vessel might pass)—we then generate the corresponding electric fields across endothelial monolayers by appropriately controlling the applied voltage to the experimental system. Both the response of individual cells and barrier integrity can be monitored as described. In this manner, we can address the hypothesis that blood vessels at specific distances from the DBS electrode may be modulated by the electric fields generated during stimulation. Further assumptions and limitations of our system are addressed in the section 4.

We also explored the possibility of the electric fields causing electro-osmosis. In separate filters, we applied the same levels of electric fields (250 V m⁻¹, 125 V m⁻¹ and 62.5 V m⁻¹) but in the absence of a hydrostatic pressure and observed if the stimulation caused any water to flow across the monolayer using the same measurement system described in section 2.5.

2.7. Immunostaining

In order to observe the effects of electric fields on the tight junctions between BAEC, the cells were stained for ZO-1. After the water flux experiments, the seeded filters were removed from the apparatus and the cells were fixed with 1% paraformaldehyde for 10 min. Following fixation, the cells were permeabilized with 0.2% Triton X-100 in PBS for 10 min and then blocked with 10% BSA and 0.1% Triton X-100 in PBS (blocking solution) for 1 h. After washing them with PBS, rabbit anti-ZO-1 diluted in the blocking solution to a final concentration of $1.25 \mu\text{g ml}^{-1}$ was added and left over night. The next day, the cells were washed five times with PBS and then incubated for 1 h with the Alexa Fluor® 488 donkey anti-rabbit secondary antibody diluted in the blocking solution to a final concentration of $4 \mu\text{g ml}^{-1}$. Once again the cells were washed four times with PBS and placed under a Nikon Eclipse TE2000-E inverted microscope for observation. Four random $20\times$ or $40\times$ fields were chosen per filter. Fluorescent images of each field were captured using a Photometrics Cascade 650 camera (Roper Scientific) connected to the microscope. Images were acquired via the MetaVue 6.2r2 imaging software (Universal Imaging) where the continuity of the ZO-1 protein at the cell junctions was observed.

2.8. Propidium iodide staining

Propidium iodide (PI) staining was carried out in order to determine the presence of dying or dead cells. Once the permeability experiments were run, the filters were rinsed with cold PBS and incubated at room temperature with a PI solution (0.001 mg ml^{-1} in PBS) for 15 min, after which the cells were rinsed once more with PBS and placed under the inverted microscope for observation.

2.9. Calcein uptake

In separate experiments, the monolayers were rinsed with warm Hank's balanced salt solution (HBSS) with Ca^{2+} and Mg^{2+} and then placed back in the incubator for 15–20 min to allow the monolayer transport resistance to recover to initial values (Ghartey-Tagoe *et al* 2004). Non-permeant calcein ($100 \mu\text{M}$) was added to the medium on the apical side of the monolayer and incubated for 5 min under controlled temperature and pH. The insert with the monolayer was then placed in the electropermeation chamber with warm 1% BSA MEM on the basal side and the same media with non-permeant calcein at a concentration of $100 \mu\text{M}$ on the apical side. Enough media was added so that the electrode was embedded in it. After stimulation with the EF, the monolayers were allowed to recover for 20 min in the incubator and then placed under the inverted microscope to observe calcein uptake. In addition, we used two positive control experiments, one where different monolayers were stimulated with 8, 12 and 14 pulses at 200 V, 1575Ω and $3275 \mu\text{F}$ using the electro cell manipulator (ECM 630, BTX Harvard Apparatus, XX). A different set of monolayers were incubated with cell permeant calcein for the second control. Both positive control experiments were followed by the same procedure to observe calcein uptake.

2.10. Statistical analysis

Water fluxes are presented as means \pm standard error (SE). The statistical analysis was made using the ANOVA function from Excel, with a Tukey–Kramer *post hoc* method, and $P < 0.05$ was considered significant. Experiments in which stimulation resulted in a more than eightfold increase in the water flux were excluded from analysis as these cases were correlated with dead cells (see section 3).

3. Results

The goal of the experimental studies was to address if the integrity of the endothelial barrier in blood vessels near DBS leads could be affected by the direct action of DBS-induced electric fields. As a first step toward addressing this question, we modeled the electric field magnitudes induced during stimulation and then applied these DBS-relevant electric fields across endothelial monolayers *in vitro* using a specially developed chamber. Both overall barrier integrity (water transport) and individual cell function (electroporation, death) were assessed. Because an *in vitro* model cannot capture the complexity of the clinical case, this experimental system was designed to address the *feasibility* of a critical clinical hypothesis, in a controlled environment where confounding variables are eliminated (see section 4).

3.1. Modeling of the electric field distribution during DBS

Finite element modeling was used to predict the electric field distribution in the tissue around energized DBS leads (figure 1). As expected, the electric field distribution depended on lead model and the electrodes energized. The iso-field contour lines (figure 3) correspond to electric field magnitudes of 250 V m^{-1} , 125 V m^{-1} and 62.5 V m^{-1} ; in each case, the cells in the tissue regions inside those contour lines would be exposed to electric fields at or greater than the respective iso-field line. Thus blood vessels traveling through these tissue regions would be exposed to these DBS-relevant electric field magnitudes. Though our homogeneous DBS model does not incorporate the implicit complexity of more detailed models (Malina *et al* 2009, Neuhaus *et al* 2008), the magnitude of changes is consistent with previous predictions. In this report, we are focused on the range of values a blood vessel traveling through the DBS electrode vicinity will encounter.

3.2. Effect of electric fields on the water flux across BAEC monolayers

The effect of DBS-relevant electric fields on the water flux across endothelial monolayers was determined. Prior to stimulation ($t = 0$ to 55 min), all the sets present an initial decrease in the water flux to a constant baseline value. This phenomenon has been observed consistently both *in vitro* and *in vivo* and has been termed 'the sealing effect' (Kim *et al* 2005). The water fluxes normalized to the sealed or baseline value (value at $t = 55$ min) are shown for each condition (figure 4). The electric fields applied at $t = 60$ min were: 250 V m^{-1} , 125 V m^{-1} or 62.5 V m^{-1} and were compared

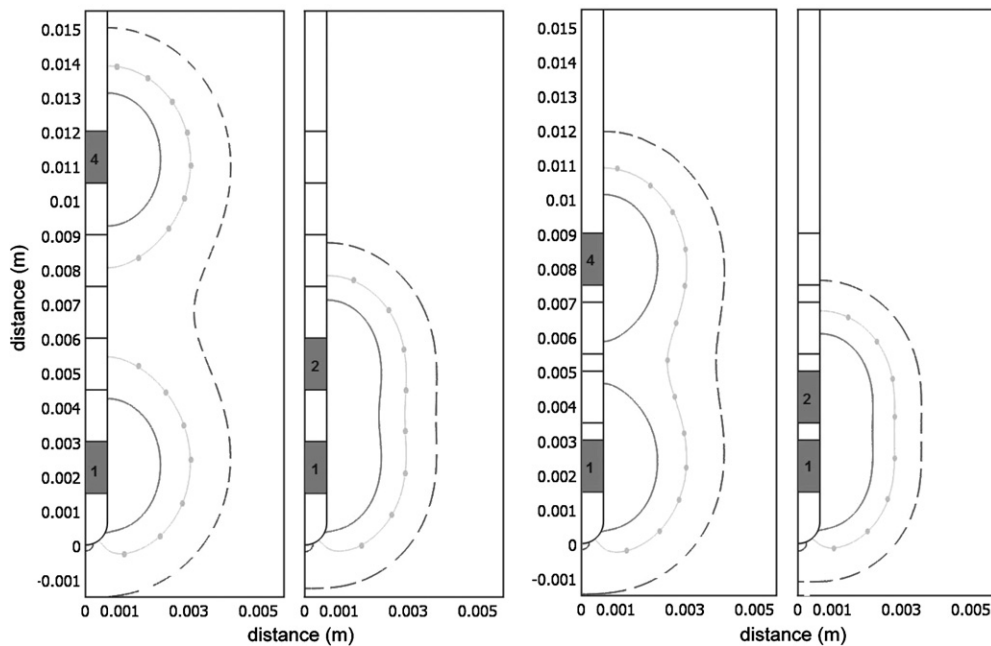


Figure 3. Electrical field profiles around DBS leads indicated as contour lines for 62.5, 125 and 250 $V m^{-1}$ (dashed line, dotted line and continuous line), respectively. A typical configuration (3 Volts) was applied in homogeneous brain tissue with electrical conductivity $\sigma = 0.3 S m^{-1}$ in both DBS leads 3387 (left) and 3389 (right) with different configurations. Electrodes 1 and 2 or electrodes 1 and 4 were electrically conductive, indicated by gray color.

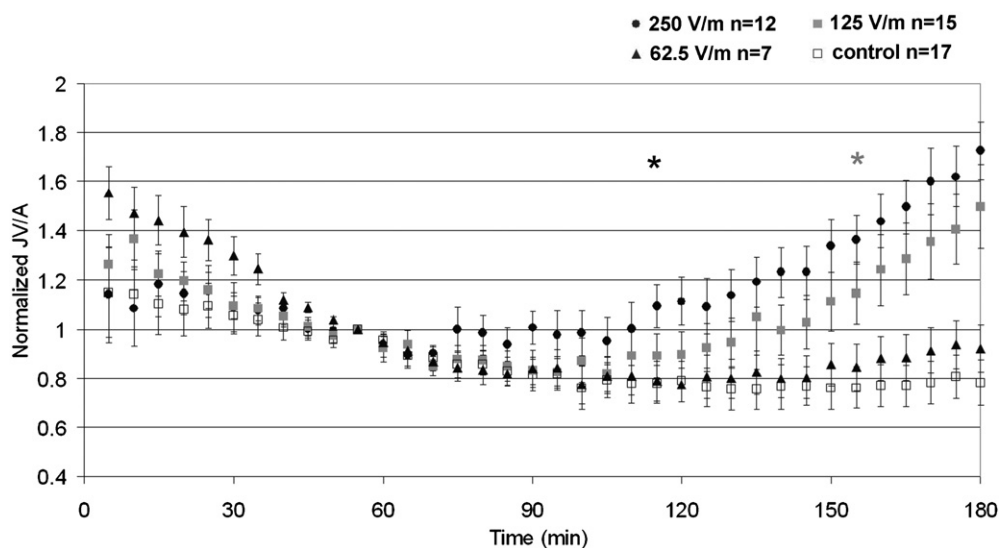


Figure 4. Normalized effect of electric field (EF) on the water flux across BAEC monolayers. The water flux, which was measured every 5 min, shows the hydraulic behavior of the monolayers. The values are normalized to the value at $t = 55$ min. During the initial 1 h incubation, the monolayers present a sealing effect and at $t = 60$ min the EF is applied for 5 min. Two hours after the EF stimulation it was evident that the hydraulic conductivity increased with the intensity of the electric field applied. Data are represented as means \pm SE ($cm s^{-1}$). The normalized values for the 250 $V m^{-1}$ curve start being significantly different from the control values at time 115 min ($p = 0.027$) and for 125 $V m^{-1}$ at time 155 min ($p = 0.031$).

to a control (no electric field applied). Stimulation with 250 $V m^{-1}$ and 125 $V m^{-1}$ electric fields increased the average water flux across the monolayers with respect to the value before the time of application (at $t = 55$ min). At the end of the experiment, a 1.73 ± 0.11 -fold increase in the water flux was observed for the electric field of 250 $V m^{-1}$ ($n = 12$) and a 1.50 ± 0.17 -fold increase for the electric field of 125 $V m^{-1}$ ($n = 15$). In contrast, the monolayers exposed to 62.5 $V m^{-1}$

($n = 7$) and not exposed at all ($n = 17$) had no significant increase in their water flux values. The ratios of the average hydraulic conductivity values for 250 $V m^{-1}$, 125 $V m^{-1}$ and 62.5 $V m^{-1}$ to control values at the end of the experiment ($t = 180$ min) were 2.22, 1.92 and 1.18, respectively.

The un-normalized values obtained for the water flux J_v/A ($cm s^{-1}$) are summarized in figure 5. The average values for the BAEC water flux obtained at $t = 55$ min

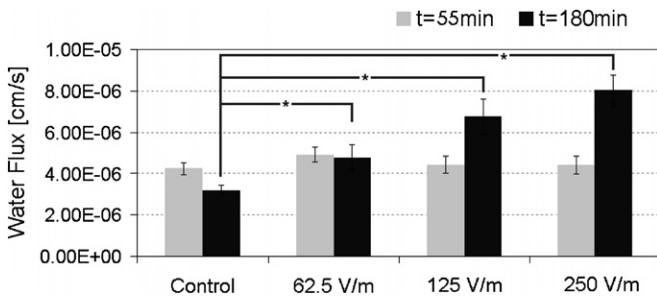


Figure 5. Effect of electric field (EF) on water flux across BAEC monolayers. Data are presented as mean \pm SE (cm s^{-1}). The different intensities of EF were applied for 5 min after 60 min of initial incubation, to bring the total experimental time to 180 min. The number of times each experimental condition was completed was as follows: control $n = 17$, 62.5 V m^{-1} $n = 7$, 125 V m^{-1} $n = 15$ and 250 V m^{-1} $n = 12$. Control experiments refer to those where no EF was applied. The values at time equal 55 min (gray bar) are not different for each set of experiments, indicating homogeneity within monolayers prior to EF application. As the field was applied, the water flux transiently increased to values that were significantly different from those of controls. At time equal 180 min (black bar), all three intensities displayed a significantly different (*) value compared to those for controls at the same time.

are in good agreement with data obtained previously in our laboratory (Cancel *et al* 2007). For each stimulated group, the corresponding controls at $t = 55$ min were not different from each other ($p = 0.742$), as expected, given that the initial condition for all the filters is the same.

The water fluxes across the monolayers exposed to all levels of EF were significantly different at $t = 180$

when compared to the values at the same time for controls (figure 5). There was a small fraction (15%) of all the monolayers that exhibited an exaggerated response to the EF; however, this response was seen after repeated use of the same electrodes and we believe it was related to chemical leaching of the electrode and subsequent chemical interaction with the cells, causing death, as these filters showed significant staining with PI. These exaggerated responses are not included in figures 4 and 5.

When we tested the monolayers to see if electro-osmosis was taking place, we observed that upon stimulation of the monolayer with a field of 250 V m^{-1} , there was flow of water across the monolayer, which was about one-tenth the magnitude of typical baseline values. This flux lasted for the amount of time the field was applied and the effect ceased when the field was removed. The fields of 125 V m^{-1} and 62.5 V m^{-1} did not induce a measurable water flux across the monolayer. This indicates that electro-osmosis had a very small and reversible contribution to water flux, which is not due to a barrier disrupting mechanism.

3.3. Effect of electric fields on ZO-1 TJ protein distribution

Fluorescent images of the ZO-1 tight-junction protein indicated that under control conditions (no stimulation by an electric field), the protein surrounds the cells continuously (figure 6(A)). In contrast, the intensity and continuity of the protein are compromised in stimulated cells. This is very apparent when comparing panels A and D. The appearance of gaps between cells is prominent at the higher field strengths.

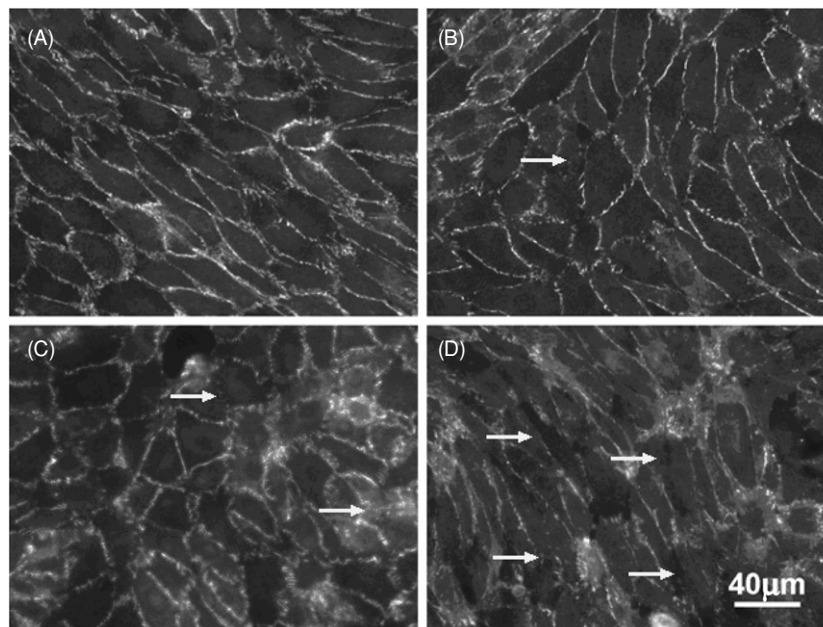


Figure 6. ZO-1 tight-junction protein staining for random frame selection of monolayers that were subjected to a pressure gradient. Upon completion of water transport experiments, the BAEC monolayers were fixed and stained for ZO-1 tight junction protein. (A) Representative staining for control (no EF). (B) Representative staining for monolayers where the EF applied was 62.5 V m^{-1} . (C) Representative staining for monolayers where the EF applied was 125 V m^{-1} . (D) Representative staining for monolayers where the EF applied was 250 V m^{-1} . Qualitatively, electric fields of 125 V m^{-1} and 250 V m^{-1} are able to modify the distribution and continuity of the protein. The arrows indicate places where discontinuities are present. The scale bar represents $40 \mu\text{m}$ for all four panels.

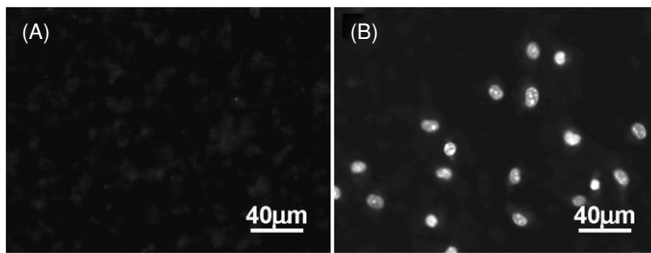


Figure 7. Propidium iodide staining of dead cells. Following the water transport experiments, monolayers were selected randomly to perform a PI staining for dead cells. Typically, neither the controls, nor the excited monolayers showed PI staining. (A) Representative staining for 250 V m^{-1} . (B) Special case in which an EF of 250 V m^{-1} caused cell death and an exceptional 41.6-fold increase in water permeability. Cell death could have been caused by chemical leaching which subsequently increased monolayer permeability.

3.4. Propidium iodide staining of electric field-induced cell death

PI staining was performed after the water flux experiments to detect any electrical stimulation-induced cell death. Results suggest that the viability of the endothelial cells is not affected by any of the DBS-relevant EF levels (62.5 V m^{-1} , 125 V m^{-1} and 250 V m^{-1}) tested in this study (figure 7(A)). In a minority of cases, and always in examples where stimulation was applied with previously used electrodes, PI staining showed dead cells. These cases were correlated with water permeability increases more than eightfold above baseline. Figure 7(B) shows a case where after stimulation with the electric field, the water flux reached a value that was 41.6 times the baseline value. This suggests that atypical and high increase in the water flux is associated with dead cells,

potentially due to electrochemical interference, and these cases were excluded from analysis (see section 2).

3.5. Calcein uptake detection of electric field-induced electroporation

We determined if DBS-relevant electric fields resulted in single cell electroporation by measuring (membrane impermeant) calcein uptake. None of the DBS-relevant fields tested in this study (62.5 V m^{-1} , 125 V m^{-1} and 250 V m^{-1}) caused significant calcein uptake (figure 8(A)). Positive controls using either membrane-permeant calcein (figure 8(B)) or membrane-impermeant calcein with high-intensity ECM stimulation ($>5000 \text{ V m}^{-1}$; we used 200 V in 4 cm) used in conventional electroporation studies (figure 8(C)–(E)) showed calcein uptake as expected. We show results for 8, 12 and 14 pulses at these high intensities; however, there was significant PI staining only for the 12 and 14 pulse cases.

4. Discussion

4.1. Assumptions and limitations of our approach

Our goal in this initial study was to determine the potential for DBS-relevant electric fields to directly modulate the integrity of the endothelial layer that forms the major transport resistance of the BBB. DBS leads and stimulation may affect BBB integrity through a range of mechanisms including mechanical damage, electrochemical interactions and indirect consequences of intense neuronal activation, but this study focused only on the direct modulation of barrier function by induced electric fields. To isolate this mechanism of action, we developed a system to apply uniform electric fields across an *in vitro* endothelial cell monolayer that was used as an

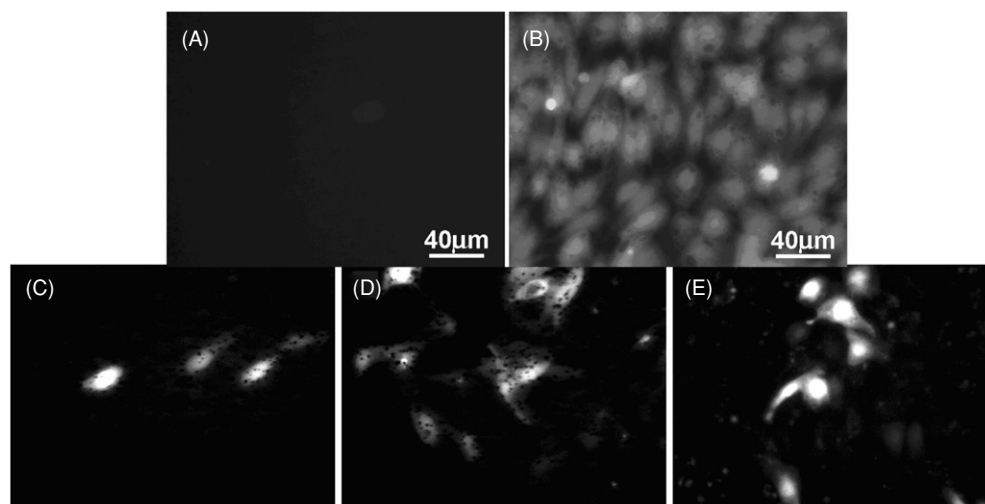


Figure 8. The BAEC monolayers were exposed for 5 min to the same levels of electric fields that were used in the measurement of water flux. Panel A on the left shows a representative picture for a monolayer stimulated with an electric field of 250 V m^{-1} , the absence of calcein uptake was also observed for the lower fields (62.5 V m^{-1} and 125 V m^{-1}). Panel B shows a positive control, where a cell-permeant calcein was used. Panels C, D and E correspond to monolayers that were exposed to pulses at 200 V , 1575Ω and $3275 \mu\text{F}$. Panel C shows the calcein uptake for a monolayer exposed to 8 pulses, panel D for a monolayer exposed to 12 pulses and panel E for a monolayer exposed to 14 pulses. The increased calcein uptake observed for 12 and 14 pulses was accompanied by significant cell death as tested by PI staining. Qualitatively, the amount of calcein taken by the cells increased as the number of pulses increased.

analog of the BBB endothelium (figure 2). The waveform of EF stimulation matched that used in conventional DBS, which is substantially different from the short pulse train used in typical electroporation studies. The magnitude of uniform EF stimulation was estimated using a FEM DBS model (figure 1). Though DBS fields are not uniform, the field may be considered uniform on the scale of an endothelial cell monolayer. The application of uniform fields resulted in all cells in the monolayer being exposed to the same known electric field. In this way, we were able to quantify the direct effects of specific DBS-relevant electric fields on single cell endothelial function, viability and transport across the monolayer. Moreover, using this system we were able to explore the mechanisms of induced changes. To our knowledge, this is the first effort to test the hypothesis that DBS might directly modulate BBB function, and despite the limitations of this initial model, we believe that our experimental results (section 3.2) are clear and the potential impact of BBB electro-permeation, should it occur in humans, is of relevance to the design of safe DBS strategies. It is important to emphasize that our results are specific to BAEC monolayers, and other *in vitro* models or BBB *in vivo* may behave differently upon stimulation.

In this study, we limited stimulation to 5 min, whereas clinical DBS is generally applied continuously. In this sense, our results may *underestimate* potential BBB modulation. We also note the potential for blood vessels to pass very near energized DBS electrodes, where the electric field magnitude increases exponentially, especially near electrode edges (Yousif and Liu 2007). This could result in higher intensity BBB stimulation than is tested in the present study. Our FEM did not incorporate all the complexity of specialized DBS models (Butson *et al* 2007, Johnson and McIntyre 2008). Among other considerations, it is worth noticing that the dynamic electrode–brain tissue interface may increase the spread of the electric fields due to the highly conductive extracellular fluid layer, but over time can also restrict it due to giant cells growing around the electrode, resulting in a resistive ‘shield’ (Yousif and Liu 2007). Our basic blood–tissue barrier model is less accurate than other specialized *in vitro* BBB systems (Vastag and Keseru 2009) and of course no *in vitro* system can fully reproduce all *in vivo* cell and environmental conditions. Incorporation of brain microvascular endothelial cells (BMVEC) or BMVEC co-cultured with astrocytes might produce a tighter BBB model that would be more resistive to DBS electric fields (Lu *et al* 2006, Demeuse *et al* 2002). However, for this initial study, we focused on the well-established and characterized BAEC model, especially as we were developing new stimulation methodology and exploring a novel mechanism.

4.2. Characteristics and mechanisms of endothelial monolayer modulation by DBS-relevant electric fields

The present study is only a first step toward elucidating the effects of EFs induced by currently used DBS protocols on the permeability of brain endothelium. In addition, as brain therapies evolve, especially as new waveforms are applied for

emerging applications and targets, new safety concerns arise. The present *in vitro* model of the endothelium of BBB has the advantage of isolating a monolayer that can be studied upon application of different electric fields. In particular, we were interested in the effects on endothelial barrier function, which is controlled by tight junctions to maintain homeostasis of the surrounding tissues.

Tight junctions limit the paracellular flux of hydrophilic molecules across the BBB and together with adherens junctions form a seal between adjacent endothelial cells, establishing cell polarity and maintaining the distinct apical and basal environments. The integrity of the TJ is in part governed by three transmembrane protein families: occludins, claudins and junctional adhesion molecules (JAMs), all of which bind to ZO-1, a 220 kDa cytoplasmic protein strongly involved in BBB TJ structure and regulation. Occludin’s carboxy-terminal binds to several zonula occluden proteins (ZO-1, ZO-2 and ZO-3) which in turn bind to the actin cytoskeleton (Fanning *et al* 1998, 2002, Furuse *et al* 1994). Claudins have two intracellular loops that bind to ZO-1, ZO-2 and ZO-3 also via their carboxy terminals (Itoh *et al* 1999), and JAMs have a single transmembrane domain which binds intracellularly to ZO-1 among other proteins (Ebnet *et al* 2003, Itoh *et al* 2001). ZO-1 therefore is a molecule that acts as a central organizer of the TJ complex.

Our results suggest that clinical levels of electric fields used in DBS could result in disruption of the endothelium, thus disrupting the first line of defense of the BBB. During our experiments, the water flux across the endothelial monolayer was significantly increased upon exposure to electric fields. This increase, which translates to an increase in hydraulic conductivity, was correlated to ZO-1 protein disorganization without any significant loss of cell viability. Increased paracellular permeability has previously been related to redistribution of actin, ZO-1 and occludin (Shen *et al* 2006) and in BBB to loss of ZO-1 and occludin at the junctions (Bolton *et al* 1998). Immunostaining of ZO-1 showed a punctuate or discontinuous pattern when the monolayers were exposed to electric fields of 125 V m^{-1} and 250 V m^{-1} (figure 6) and we believe that this tight-junction breakdown is the main cause of significantly elevated hydraulic conductivity. However, as the TJ is formed by a complex structure of several proteins, a more detailed screening of proteins will be required to thoroughly understand this phenomenon. We chose to focus our attention on ZO-1 as it constitutes a central anchoring protein for the TJ complex. In the past, adherens junctions and the cytoskeleton have been shown to be disrupted due to stimulation by electric fields used in electroporation, both of which could result in increased endothelial permeability (Kanthou *et al* 2006).

Our experiments also show that the monolayers did not recover their barrier function during the 2 h postapplication of the electric field; however, *in vivo* conditions may differ and further investigation in animals will be important in determining if there is a recovery time for these EF levels and the extent to which this recovery time could be harmful to brain tissue. *In vivo*, electrical stimulation of cat cortex has demonstrated an increased permeability of the BBB as estimated by extravasation of trypan blue (Mortimer *et al*

1970) with recovery periods of up to 4 weeks. Others have also shown endothelial disruption in cat brain parenchymal capillaries upon electrical stimulation (Agnew *et al* 1975). In our model system, the absence of neuronal cells indicates a direct blood barrier response to stimulation.

Interestingly, the electric fields applied in our study did not induce single cell electroporation, as calcein was not taken up into the cytosol (figure 8). DBS-relevant electric fields may thus be below the threshold for membrane pore formation. In our positive controls using electric fields of 5000 V m^{-1} , calcein uptake was observed as well as cell death. It has been shown before that not only the EF amplitude, but also the composition of the membrane and the location of the sites of the initial field-driven water flux into the bilayer are relevant parameters in electroporation (Ziegler and Vernier 2008). It is important to emphasize that the same electric fields that increased hydraulic conductivity in the monolayers did not cause cell membrane electroporation, suggesting that loss of endothelium barrier integrity may precede single cell electroporation. Barrier electro-permeation may thus occur at lower stimulation intensities and/or at farther distances from the electrodes as single cell electroporation.

4.3. Proposed remedial safety measures

Certainly the result of this *in vitro* study must be interpreted cautiously in regard to the clinical situation. Even with the limitations of the present model, our results clearly demonstrate the possibility of BBB disruption by DBS-induced electric fields. Therefore, based on our initial results and the potential impact of BBB disruption on DBS safety, further investigation in more complex animal models and eventual clinical studies appear warranted.

Acknowledgments

This study was supported by NHLBI grant HL-57093 and NIH S06GMOO8168.

References

- Agnew W F, Yuen T G, Pudenz R H and Bullara L A 1975 Electrical stimulation of the brain. Ultrastructural studies *Surg. Neurol.* **4** 438–48
- Anwar M and Weiss HR 1989 Adenosine and cerebral capillary perfusion and blood flow during middle cerebral artery occlusion *Am. J. Physiol.* **257** (Pt 2) H1656–62
- Bekar L *et al* 2008 Adenosine is crucial for deep brain stimulation-mediated attenuation of tremor *Nat. Med.* **14** 75–80
- Benabid A L 2007 What the future holds for deep brain stimulation *Expert Rev. Med. Devices* **4** 895–903
- Bikson M, Inoue M, Akiyama H, Deans J K, Fox J E, Miyakawa H and Jefferys J G 2004 Effects of uniform extracellular DC electric fields on excitability in rat hippocampal slices *in vitro* *J. Physiol.* **557** (Pt 1) 175–90
- Bikson M, Lian J, Hahn P J, Stacey W C, Sciortino C and Durand D M 2001 Suppression of epileptiform activity by high frequency sinusoidal fields in rat hippocampal slices *J. Physiol.* **531** (Pt 1) 181–91
- Bolton S J, Anthony D C and Perry V H 1998 Loss of the tight junction proteins occludin and zonula occludens-1 from cerebral vascular endothelium during neutrophil-induced blood–brain barrier breakdown *in vivo* *Neuroscience* **86** 1245–57
- Butson C R, Cooper S E, Henderson J M and McIntyre C C 2007 Patient-specific analysis of the volume of tissue activated during deep brain stimulation *Neuroimage* **34** 661–670
- Butson C R and McIntyre C C 2005 Tissue and electrode capacitance reduce neural activation volumes during deep brain stimulation *Clin. Neurophysiol.* **116** 2490–500
- Cancel L M, Fitting A and Tarbell J M 2007 *In vitro* study of LDL transport under pressurized (convective) conditions *Am. J. Physiol. Heart Circ. Physiol.* **293** H126–32
- Chang Y S, Yaccino J A, Lakshminarayanan S, Frangos J A and Tarbell J M 2000 Shear-induced increase in hydraulic conductivity in endothelial cells is mediated by a nitric oxide-dependent mechanism *Arterioscler. Thromb. Vasc. Biol.* **20** 35–42
- Chou Y C, Lin S Z, Hsieh W A, Lin S H, Lee C C, Hsin Y L, Yen P S, Lee C W, Chiu W T and Chen S Y 2007 Surgical and hardware complications in subthalamic nucleus deep brain stimulation *J. Clin. Neurosci.* **14** 643–9
- Datta A, Tarbell J M and Bikson M 2007 Electroporation of endothelial cells by high frequency electric fields: implications for DBS *Bioengineering Conf. Procedures of the IEEE 33rd Annual Northeast* pp 138–9
- DeMaio L, Tarbell J M, Scaduto R C Jr, Gardner T W and Antonetti D A 2004 A transmural pressure gradient induces mechanical and biological adaptive responses in endothelial cells *Am. J. Physiol. Heart Circ. Physiol.* **286** H731–41
- Demeuse P, Kerkhofs A, Struys-Ponsar C, Knoops B, Remacle C and Van Den Bosch de Aguilar P 2002 Compartmentalized coculture of rat brain endothelial cells and astrocytes: a syngenic model to study the blood–brain barrier *J. Neurosci. Methods* **121** 21–31
- Drapier D *et al* 2008 Emotion recognition impairment and apathy after subthalamic nucleus stimulation in Parkinson's disease have separate neural substrates *Neuropsychologia* **46** 2796–801
- Ebnet K, Aurrand-Lions M, Kuhn A, Kiefer F, Butz S, Zander K, Meyer zu Brickwedde M K, Suzuki A, Imhof BA and Vestweber D 2003 The junctional adhesion molecule (JAM) family members JAM-2 and JAM-3 associate with the cell polarity protein PAR-3: a possible role for JAMs in endothelial cell polarity *J. Cell Sci.* **116** (Pt 19) 3879–91
- Elwassif M M, Kong Q, Vazquez M and Bikson M 2006 Bio-heat transfer model of deep brain stimulation-induced temperature changes *J. Neural Eng.* **3** 306–15
- Fanning A S, Jameson B J, Jesaitis L A and Anderson J M 1998 The tight junction protein ZO-1 establishes a link between the transmembrane protein occludin and the actin cytoskeleton *J. Biol. Chem.* **273** 29745–53
- Fanning A S, Ma T Y and Anderson J M 2002 Isolation and functional characterization of the actin binding region in the tight junction protein ZO-1 *Faseb J.* **16** 1835–7
- Furuse M, Itoh M, Hirase T, Nagafuchi A, Yonemura S, Tsukita S and Tsukita S 1994 Direct association of occludin with ZO-1 and its possible involvement in the localization of occludin at tight junctions *J. Cell. Biol.* **127** (Pt 1) 1617–26
- Ghartey-Tagoe E B, Morgan J S, Ahmed K, Neish A S and Prausnitz M R 2004 Electroporation-mediated delivery of molecules to model intestinal epithelia *Int. J. Pharm.* **270** 127–38
- Gluckman B J, Neel E J, Netoff T I, Ditto W L, Spano M L and Schiff S J 1996 Electric field suppression of epileptiform activity in hippocampal slices *J. Neurophysiol.* **76** 4202–5
- Hardesty D E and Sackeim H A 2007 Deep brain stimulation in movement and psychiatric disorders *Biol. Psychiatry* **61** 831–5
- Hawkins B T and Davis T P 2005 The blood–brain barrier/neurovascular unit in health and disease *Pharmacol. Rev.* **57** 173–85

- Jensen J H, Hanzhang L and Inglese M 2006 Microvessel density estimation in the human brain by means of dynamic contrast-enhanced echo-planar imaging *Magn. Reson. Med.* **56** 1145–50
- Itoh M, Furuse M, Morita K, Kubota K, Saitou M and Tsukita S 1999 Direct binding of three tight junction-associated MAGUKs, ZO-1, ZO-2, and ZO-3, with the COOH termini of claudins *J. Cell Biol.* **147** 1351–63
- Itoh M, Sasaki H, Furuse M, Ozaki H, Kita T and Tsukita S 2001 Junctional adhesion molecule (JAM) binds to PAR-3: a possible mechanism for the recruitment of PAR-3 to tight junctions *J. Cell Biol.* **154** 491–7
- Johnson M D and McIntyre C C 2008 Quantifying the neural elements activated and inhibited by globus pallidus deep brain stimulation *J. Neurophysiol.* **100** 2549–63
- Kanthou C, Kranjc S, Sersa G, Tozer G, Zupanic A and Cemazar M 2006 The endothelial cytoskeleton as a target of electroporation-based therapies *Mol. Cancer Ther.* **5** 3145–52
- Khine M, Ionescu-Zanetti C, Blatz A, Wang L P and Lee L P 2007 Single-cell electroporation arrays with real-time monitoring and feedback control *Lab Chip* **7** 457–62
- Kim M H, Harris N R and Tarbell J M 2005 Regulation of hydraulic conductivity in response to sustained changes in pressure *Am. J. Physiol. Heart Circ. Physiol.* **289** H2551–8
- Kuyck K V, Welkenhuysen M, Arckens L, Sciort R and Nuttin B 2007 Histological alterations induced by electrode implantation and electrical stimulation in the human brain: a review *Neuromodulation: Technol. Neural Interface* **10** 244–61
- Lakshminarayanan S, Gardner T W and Tarbell J M 2000 Effect of shear stress on the hydraulic conductivity of cultured bovine retinal microvascular endothelial cell monolayers *Curr. Eye Res.* **21** 944–51
- Larson P S 2008 Deep brain stimulation for psychiatric disorders *Neurotherapeutics* **5** 50–8
- Lipsman N, Neimat J S and Lozano A M 2007 Deep brain stimulation for treatment-refractory obsessive-compulsive disorder: the search for a valid target *Neurosurgery* **61** 1–11 (discussion 11–3)
- Lu W, Tan Y Z and Jiang X G 2006 Establishment of coculture model of blood–brain barrier *in vitro* for nanoparticle's transcytosis and toxicity evaluation *Yao Xue Xue Bao* **41** 296–304
- Malina K C, Cooper I and Teichberg V I 2009 Closing the gap between the *in-vivo* and *in-vitro* blood–brain barrier tightness *Brain Res.* **1284** 12–21
- McClelland S III, Ford B, Senatus P B, Frucht S J, Winfield L M, Yu Q, Du Y E, Pullman S L, McKhann G M II and Goodman R R 2009 Typical variations of subthalamic electrode location do not predict limb motor function improvement in Parkinson's disease *J. Clin. Neurosci.* **16** 771–8 (discussion 779)
- Merrill D R, Bikson M and Jefferys J G 2005 Electrical stimulation of excitable tissue: design of efficacious and safe protocols *J. Neurosci. Methods* **141** 171–98
- Mortimer J T, Shealy C N and Wheeler C 1970 Experimental nondestructive electrical stimulation of the brain and spinal cord *J. Neurosurg.* **32** 553–9
- Moss J, Ryder T, Aziz T Z, Graeber M B and Bain P G 2004 Electron microscopy of tissue adherent to explanted electrodes in dystonia and Parkinson's disease *Brain* **127** (Pt 12) 2755–63
- Neuhaus W, Plattner V E, Wirth M, Germann B, Lachmann B, Gabor F and Noe C R 2008 Validation of *in vitro* cell culture models of the blood–brain barrier: tightness characterization of two promising cell lines *J. Pharm. Sci.* **97** 5158–75
- Pucihar G, Kotnik T, Teissie J and Miklavcic D 2007 Electroporation of dense cell suspensions *Eur. Biophys. J.* **36** 173–85
- Radman T, Su Y, An J H, Parra L C and Bikson M 2007 Spike timing amplifies the effect of electric fields on neurons: implications for endogenous field effects *J. Neurosci.* **27** 3030–6
- Rebersek M, Faurie C, Kanduser M, Corovic S, Teissie J, Rols M P and Miklavcic D 2007 Electroporator with automatic change of electric field direction improves gene electrotransfer *in-vitro Biomed. Eng. Online* **6** 25
- Sani S, Jobe K, Smith A, Kordower J H and Bakay R A 2007 Deep brain stimulation for treatment of obesity in rats *J. Neurosurg.* **107** 809–13
- Shen L, Black E D, Witkowski E D, Lencer W I, Guerriero V, Schneeberger E E and Turner J R 2006 Myosin light chain phosphorylation regulates barrier function by remodeling tight junction structure *J. Cell. Sci.* **119** (Pt 10) 2095–106
- Sill H W, Chang Y S, Artman J R, Frangos J A, Hollis T M and Tarbell J M 1995 Shear stress increases hydraulic conductivity of cultured endothelial monolayers *Am. J. Physiol.* **268** (Pt 2) H535–43
- Stacey M, Stickley J, Fox P, Statler V, Schoenbach K, Beebe S J and Buescher S 2003 Differential effects in cells exposed to ultra-short, high intensity electric fields: cell survival, DNA damage, and cell cycle analysis *Mutat. Res.* **542** 65–75
- Sun D A, Yu H, Spooner J, Tatsas A D, Davis T, Abel T W, Kao C and Konrad P E 2008 Postmortem analysis following 71 months of deep brain stimulation of the subthalamic nucleus for Parkinson disease *J. Neurosurg.* **109** 325–9
- Tir M *et al* 2007 Exhaustive, one-year follow-up of subthalamic nucleus deep brain stimulation in a large, single-center cohort of parkinsonian patients *Neurosurgery* **61** 297–304 (discussion 304–295)
- Vastag M and Keseru G M 2009 Current *in vitro* and *in silico* models of blood–brain barrier penetration: a practical view *Curr. Opin. Drug. Discov. Devel.* **12** 115–24
- Voges J, Koulousakis A and Sturm V 2007 Deep brain stimulation for Parkinson's disease *Acta Neurochir. Suppl.* **97** (Pt 2) 171–84
- Yang T A, Heiser W C and Sedivy J M 1995 Efficient *in situ* electroporation of mammalian cells grown on microporous membranes *Nucleic Acids Res.* **23** 2803–10
- Yousif N and Liu X 2007 Modelling the current distribution across the depth electrode–brain interface in deep brain stimulation *Expert Rev. Med. Devices* **4** 623–31
- Ziegler M J and Vernier P T 2008 Interface water dynamics and porating electric fields for phospholipid bilayers *J. Phys. Chem. B* **112** 13588–96